

Spatial patterns of simulated transpiration response to climate variability in a snow dominated mountain ecosystem

Lindsey Christensen,^{1*} Christina L. Tague² and Jill S. Baron³

¹ *Natural Resource Ecology Laboratory, Colorado State University, Fort Collins, CO, USA*

² *Donald Bren School of Environmental Science & Management, University of California, Santa Barbara, CA, USA*

³ *US Geological Survey, Natural Resource Ecology Laboratory, Colorado State University, Fort Collins, CO, USA*

Abstract:

Transpiration is an important component of soil water storage and stream-flow and is linked with ecosystem productivity, species distribution, and ecosystem health. In mountain environments, complex topography creates heterogeneity in key controls on transpiration as well as logistical challenges for collecting representative measurements. In these settings, ecosystem models can be used to account for variation in space and time of the dominant controls on transpiration and provide estimates of transpiration patterns and their sensitivity to climate variability and change. The Regional Hydro-Ecological Simulation System (RHESSys) model was used to assess elevational differences in sensitivity of transpiration rates to the spatiotemporal variability of climate variables across the Upper Merced River watershed, Yosemite Valley, California, USA. At the basin scale, predicted annual transpiration was lowest in driest and wettest years, and greatest in moderate precipitation years ($R^2 = 0.32$ and 0.29 , based on polynomial regression of maximum snow depth and annual precipitation, respectively). At finer spatial scales, responsiveness of transpiration rates to climate differed along an elevational gradient. Low elevations (1200–1800 m) showed little interannual variation in transpiration due to topographically controlled high soil moistures along the river corridor. Annual conifer stand transpiration at intermediate elevations (1800–2150 m) responded more strongly to precipitation, resulting in a unimodal relationship between transpiration and precipitation where highest transpiration occurred during moderate precipitation levels, regardless of annual air temperatures. Higher elevations (2150–2600 m) maintained this trend, but air temperature sensitivities were greater. At these elevations, snowfall provides enough moisture for growth, and increased temperatures influenced transpiration. Transpiration at the highest elevations (2600–4000 m) showed strong sensitivity to air temperature, little sensitivity to precipitation. Model results suggest elevational differences in vegetation water use and sensitivity to climate were significant and will likely play a key role in controlling responses and vulnerability of Sierra Nevada ecosystems to climate change. Copyright © 2008 John Wiley & Sons, Ltd.

KEY WORDS spatial modeling; climate variability; transpiration; Merced River; RHESSys; hydrologic simulations; Yosemite National Park

Received 8 December 2006; Accepted 25 October 2007

INTRODUCTION

Mountains are the primary source of western US water. Understanding hydrologic patterns in these environments is important for the assessment of water resources, ecological function, and the socio-economic implications of changes to these systems (Dirnböck and Grabherr, 2000; Shär and Frei, 2005). Before mountain precipitation flows into the stream network, it is subject to storage as groundwater and snow, and loss due to evaporation, sublimation, and transpiration (Mote *et al.*, 2005; van Lier *et al.*, 2005). In much of the mountain western US, plant transpiration is a significant component of the water budget and is a controlling factor of the underlying hydrologic cycle (Wilson *et al.*, 2001; Shär and Frei, 2005). Understanding controls of and variability in watershed transpiration is important not only for estimation of total water budgets, but also for the role

of transpiration in energy budgets (Nishida *et al.*, 2003) and understanding effects of hydrological flows on carbon source/sink dynamics (Nemani *et al.*, 2002) and how these systems might respond to climate change (Bales *et al.*, 2006).

Climate change is projected to significantly alter the hydrology of western US mountain ecosystems, primarily as a result of increased temperatures, reductions in snow accumulation, and earlier snow melt (Pupacko, 1993; Dettinger and Cayan, 1995; Dettinger *et al.*, 2004; Stewart, 2004). Summer soil moisture will likely be reduced, leaving systems vulnerable to reductions in net primary production, increased fire frequency, and changes in vegetation types (Loik *et al.*, 2000; Bachelet *et al.*, 2001; Dale *et al.*, 2001; Pan *et al.*, 2004). Understanding the spatiotemporal trends of transpiration within a watershed will allow for better estimates of the current distributed water balance and how these systems might respond to climate variations (Eder *et al.*, 2005; Gurtz *et al.*, 2005; Shär and Frei, 2005; van Lier *et al.*, 2005; Boisvenue and Running, 2006).

*Correspondence to: Lindsey Christensen, Natural Resource Ecology Laboratory, Colorado State University, Fort Collins, CO 80523-1499, USA. E-mail: lindsey@nrel.colostate.edu

In mountain environments, spatial patterns of transpiration reflect interactions between topographic controls on energy, moisture availability, and vegetation biomass and species. Significant heterogeneity in transpiration is common given large elevation and aspect gradients that influence both atmospheric conditions and soil moisture and groundwater redistribution (Whitaker *et al.*, 2003; Kane, 2005; van Lier *et al.*, 2005). Weather patterns are extremely variable in mountain ecosystems due to large differences in elevations and complex topography resulting in variable precipitation, wind, and air temperature patterns (Barry, 1992; Kane, 2005; Kang *et al.*, 2006). Plant function is closely related to these hydroclimatological patterns (Kang *et al.*, 2006). Along with spatial variability is interannual variability in transpiration rates, driven by fluctuating climate patterns. In mountainous regions, the relative rarity of weather stations, limited monitoring resources in remote areas, and access difficulties make quantifying spatial-temporal patterns of transpiration a key research challenge (Diaz, 2005; van Lier *et al.*, 2005).

Spatially explicit models can be used to address hydrological questions in the complex terrain of mountain ecosystems (Whitaker *et al.*, 2003). While models are inherently uncertain and cannot substitute for direct field measurements, they provide a tool for estimating how multiple, interacting controls may influence spatial-temporal patterns of transpiration. Models serve to generate hypotheses about where significant differences in climate-transpiration relationships are likely to be observed; they can then be used to guide efficient field monitoring campaigns. In this paper, we used a process-based ecosystem model, Regional Hydro-Ecological Simulation System (RHESys), to simulate the spatiotemporal response of transpiration to climate for the Upper Merced River watershed in Yosemite Valley, California (Tague and Band, 2004). Transpiration water loss is an important component of the Upper Merced basin's hydrological flow. This basin loses approximately 40% of annual precipitation to evapotranspiration, 77% of which is estimated as transpiration (Clow *et al.*, 1996). By focusing on spatial variation of watershed transpiration, an insight can be shown into the details of water distribution through a watershed with variable terrain and the causes of spatial differences in the relationship between transpiration and climate forcing. With this model, three questions can be addressed: (1) how do air temperature and precipitation variability affect transpiration in a high elevation mountain ecosystem at a basin wide scale, (2) how does transpiration vary with elevation within a basin, and (3) at separate elevations, what are the drivers that cause this variability and how do they differ temporally and spatially? These model results present process-based hypotheses about the spatial structure of transpiration responses to climate variability that can guide interpretation of basin-scale ecosystem and hydrologic behaviour under past and future climate trajectories and serve as a template to design future field-based monitoring.

METHODS

Site Description

The upper Merced River watershed is a 465 km² basin located on the western slope of the Sierra Nevada Mountains, in Yosemite National Park (Figure 1), ranging in elevation from 1220 m at the Happy Isles Bridge stream gauge to the summit of Mount Lyell at 3997 m (Mast and Clow, 2000). Annual average minimum and maximum daily air temperatures for water years (defined as October through September) 1926 to 2003 are 3.9 and 20.2 °C, respectively, with maximum annual high air temperature at 23.6 °C and annual low at 1.5 °C, measured at the National Climate Data Centre Yosemite Headquarters station, located 3.0 km north-west of the stream gauge (station 49 855, <http://wf.ncdc.noaa.gov/oa/ncdc.html>). The mean annual precipitation for water years 1926 to 2003 was 88.9 cm, and ranged from 29.3 to 166.5 cm. The upper Merced basin is snow dominated, with snowpack occurring from October to April and snowmelt occurring from April to June (Mast and Clow, 2000). From 1926–2003, average annual discharge, normalized by drainage area, was 67.4 cm but ranged from 16.7 to 154.2 cm.

Conifers are the dominant vegetation type within the watershed (68.5%) and include pines (*Pinus contorta*, *P. ponderosa*, *P. jeffreyi*, *P. monticola*, and *P. albicaulis*), fir (*Abies magnifica* and *A. concolor*), hemlock (*Tsuga mertensiana*), Douglas fir (*Pseudotsuga menziesii*), and juniper (*Juniperus scopulorum*). Deciduous trees make up less than 1% of the watershed, and include *Acer sp.* and *Quercus sp.* Other vegetation includes shrubs (including willow), sedges, and



Figure 1. Yosemite National Park with three-dimensional inlay of upper Merced River Basin

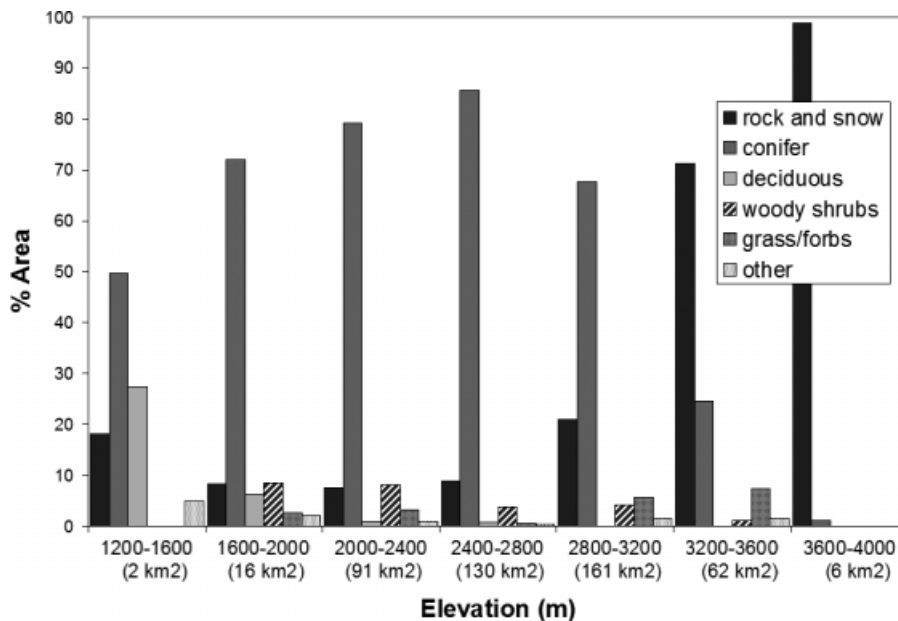


Figure 2. Proportion of vegetation type within elevation regions of the upper Merced watershed. The total area associated with each elevation region is located in parenthesis

forbs, totaling 6% of the watershed. The remainder is classified as rock outcrop (Aerial Information System, 2003). Figure 2 summarizes the distribution of vegetation types within specific elevation ranges of the watershed. Soils are primarily Inceptisols with sandy loam (Mast and Clow, 2000) and loamy sand texture (STATSGO, <http://www.ncgc.nrcs.usda.gov/products/datasets/statsgo>).

Model description

RHESSys (Band *et al.*, 1993, 1996; Tague and Band, 2001, 2004) is a spatially distributed, dynamic model of water, carbon, and nitrogen fluxes over spatially variable terrain ranging from tens to hundreds of kilometres. RHESSys was chosen based on its ability to simulate interactions between these fluxes and climate patterns within a mountainous environment. Here RHESSys version 5.12 is used, which incorporates a climate interpolation model (MT-CLIM; Running *et al.*, 1987), a vegetation and soil nutrient cycling model (adapted and extended from BIOME-BGC; Thornton, 1998), and models of vertical and lateral hydrologic fluxes. Detailed description of these models is provided in Tague and Band (2004).

RHESSys uses a hierarchical spatial framework that allows different processes to be modelled at their most representative scale (Band *et al.*, 2001). The largest spatial division is the basin, defined as a hydrologically closed drainage area encompassing a single stream network. Basins are divided into hillslopes, areas that drain into one side of a single stream reach, delineated using a GIS-basin partitioning algorithm in the Geographic Resources Analysis Support System (GRASS) (<http://grass.itc.it/index.php>). Zones, which describe areas of similar climate, represent the next smaller division. Explicit routing of hydrological flows is organized within

hillslopes. Patches are the smallest spatial unit wherein vertical soil moisture and biogeochemistry are modelled, and are defined as areas of similar soil moisture and land-cover characteristics.

Daily minimum and maximum air temperatures and precipitation drive biogeochemical cycling and hydrologic flux estimates. Spatial inputs of both air temperature and dewpoint are adjusted by a lapse rate (0.0064 and 0.0015 °C m⁻¹, respectively) with elevation. Meteorological variables, including radiation (diffuse and direct), partitioning of rain and snow, saturation vapour pressure, and relative humidity, are simulated for each zone. Variation in these meteorological variables with topography is based on algorithms from the MT-CLIM model (Running *et al.*, 1987). The ecophysiological component of RHESSys is adapted from BIOME-BGC (Thornton, 1998) and Century (Parton *et al.*, 1996), with refinements in sub-models of overstory and understory canopy light interception, litter moisture storage and evaporation, carbon allocation, and canopy impacts on snowmelt (Tague and Band, 2004). The model estimates gross photosynthesis and respiration, allocates net photosynthesis to leaves, stems, and roots, and assumes a mature forest stand. Soil decomposition and nitrification and denitrification processes are also simulated. The hydrologic component of RHESSys is described in more detail later.

Input and simulated meteorological variables and stand structure (LAI, canopy height, species-specific parameters) are used to estimate canopy radiative and moisture fluxes, as well as vegetation carbon and nitrogen cycling. Species specific vegetation parameters are available as standard RHESSys libraries, and are assigned based on a vegetation type map. Detailed description of all process sub-models is beyond the scope of this paper and the reader is referred to Tague and Band (2004). Here key sub-models used in the estimation of transpiration

are summarized. Evaporation and sublimation of intercepted water, transpiration, and soil and litter evaporation are computed using the Penman–Monteith algorithm (Monteith, 1965). To calculate stomatal conductance, RHESSys uses the Jarvis model (Jarvis, 1976) where maximum conductance (a vegetation input parameter) is scaled by environmental factors, including light, CO₂, predawn leaf water potential (computed as a function of soil moisture), air temperature, and vapour pressure deficit. The aerodynamic conductance terms are computed as a function of canopy height and wind speed, following (Heddeland and Lettenmaier, 1995). Wind-speed data was not available for the basin, so a minimal value was set at 1 m s⁻¹. While it is acknowledged that spatial variation in wind speed may be an important driver in mountain environments, detailed measurements are not available to quantify these patterns. Thus, the model depicts how interactions between spatial patterns of soil moisture, radiation, air temperature, vapour pressure deficit, and vegetation stand structure influence spatial-temporal patterns of transpiration.

RHESSys uses a three-layer model to simulate vertical soil moisture fluxes, which includes surface detention, unsaturated, and saturated stores in addition to a seasonal snowpack. The mass balance of moisture in the vertical flux includes drainage from the unsaturated layer, capillary rise, infiltration, evapotranspiration, and snowmelt, with storage in the unsaturated, saturated, and surface detention stores. Lateral fluxes of saturated zone and surface water are functions of topography and soil hydraulic conductivity following an approach used by the Distributed Hydrology Soil Vegetation Model (DHSVM) (Wigmosta *et al.*, 1994).

The version of RHESSys used in this study (5.13b) includes both surface and subsurface storage and routing (Tague and Band, 2003) and a deep groundwater store, defined at the hillslope level (Tague *et al.*, 2008). A fixed percentage of infiltrated water is assumed to bypass the soil matrix to the deep groundwater store and this store is assumed to be a linear reservoir. The percentage of bypass flow and a drainage constant for the deep groundwater store are calibrated parameters, as described later. In this study, the combined use of a deep groundwater store and shallow subsurface stores and routing effectively partitions recharge into local and spatially redistributed soil water that is accessible by plants and water that bypasses the soil matrix, and drains, to the stream. Given the goal of estimating transpiration patterns, it is argued that the simple linear reservoir model for deep groundwater is sufficient and it is not necessary to model the complex flowpath and residence time distributions associated with fractured bedrock and spring systems associated with the deep groundwater storage in the Sierra (Rademacher *et al.*, 2001).

Model Inputs

Continuous stream-flow data for the upper Merced watershed were obtained from the US Geological Survey

Hydrological Benchmark (HBM) Network at the Happy Isles Bridge (<http://waterdata.usgs.gov/nwis/discharge>, station USGS11264500, from 1923 to 2003). Daily minimum and maximum air temperatures and precipitation data from the National Climatic Data Centre (NCDC) for Yosemite Park Headquarters (station ID 49855) were used. To account for spatial variation in precipitation across the watershed, we used 2.5 arc minute (~4 km) PRISM data (PRISM Group, Oregon State University, <http://www.prismclimate.org>, created 4 February 2004) to derive a map of multipliers (proportion map) to be applied to meteorological station precipitation data. Multipliers were computed as the ratio of mean annual precipitation at the meteorological station to the PRISM estimates of mean annual precipitation at each RHESSys zone. Spatial delineation of zones is described later. The climate sub-model uses this map to scale precipitation data from the meteorological station and provide precipitation inputs for each zone.

RHESSys uses vegetation, soil, and Digital Elevation Model (DEM) maps for the spatial analyses of carbon, nitrogen, and hydrological processes. The base soil map was derived from the State Soil Geographic (STATSGO, <http://www.ncgc.nrcs.usda.gov/products/datasets/statsgo>) database. Pedon data collected by the National Soil Survey Characterization Data were used to verify soil types (e.g. sandyloam) (NSSCD, 2006). The coarse-scale (1:250 000) STATSGO data were supplemented with information from a finer-scale vegetation map created using 1997 aerial photography (Aerial Information Systems, 2003), which identified rock, talus, scree, and dome locations typical of this region. Rock, talus, scree and soils (loamy sand and sandyloam) are differentiated by their saturation hydraulic conductivity (0.0001, 10.0, 10.0, 3.0 m day⁻¹, respectively). Rock and scree have been shown to contain unique water holding capacities in upper elevation ecosystems (Clow *et al.*, 2003), however this level of detail is not incorporated into this model analysis. Soil parameters for each soil type were taken from RHESSys parameter libraries (<http://fiesta.bren.ucsb.edu/~rhessys/index.html>).

The vegetation species map of Yosemite (Aerial Information Systems, 2003) was modified to create 11 vegetation types based on similar functional groups or species (from the original 19) in the upper Merced watershed (see Appendix A). The vegetation types were linked with vegetation ecophysiological characteristics from existing RHESSys parameter libraries, with additional contributions from plant physiological research (White *et al.*, 2000).

RHESSys was used to compute vegetation carbon stores and associated leaf area index (LAI), which influence transpiration estimates. Initial simulations found significant over-estimation of LAI in many areas of the watershed based on a comparison with MODIS (Moderate Resolution Imaging Spectroradiometer) LAI products for 2004. Areas of overestimated LAI from within RHESSys simulations were identified as areas dominated by rock outcropping, geologic domes, and talus fields,

which were at too fine a resolution to be identified in vegetation and soil maps. To account for this, MODIS LAI was used to initialize LAI at the start of the simulations to more accurately represent the amount of forested area. RHESSys then modelled year-to-year variation in growth trajectories of this initial LAI.

The 30-m DEM (SNEP, 2005) was used to create slope, aspect, streams, and the spatial hierarchical network (described previously) using a GIS-based terrain partitioning algorithm in the GRASS environment. Hillslopes were defined using a drainage area threshold of 9 km (e.g. hillslopes are areas draining either side of a stream reach, given a stream network defined using this drainage area threshold). Hillslopes were further divided into zones using 100-m elevation bands, totalling 6634 zones. Hillslopes, 100-m elevation bands, and streams were used to delineate patches, the smallest unit in the spatial hierarchy. The created patch map was then recategorized in GRASS (http://grass.itc.it/announces/announce_grass620.html) by grouping neighbouring cells that form physically discrete areas into unique categories, which totalled 2457 patches.

Model Calibration and Analysis

Prior to calibration and model analyses, RHESSys was run for 2520 years until soil carbon and nitrogen pools were stabilized (pools were initialized at 0 g m^{-2}). Sixty-nine years of climate data (1926–1995) were repeated to create weather sequences for this initial run. Once carbon and nitrogen pools were in equilibrium, the model was calibrated against observed stream-flow to determine values of input parameters including: saturated hydraulic conductivity (K), decay of K with depth (m) (representing total soil transmissivity), the fraction of recharge that bypasses shallow subsurface flow system to deeper groundwater store (gw1) and drainage rate of deeper groundwater store (gw2). A Monte Carlo approach was used to sample over a joint distribution of m , K , gw1, and gw2 values and select the parameter set yielding optimal performance as measured by comparisons between observed and simulated stream-flow. Calibrations included 500 simulations of a 10-year period, 1980–1989. Performance metrics used to evaluate the correspondence between observed and modelled stream-flow include the error in mean annual stream-flow estimates and the Nash–Sutcliffe efficiency (Nash and Sutcliffe, 1970) between observed and modelled flow using daily and log-transformed daily stream-flows.

An optimal parameter set based on the performance metrics outlined earlier was selected and used for subsequent model validation and analyses. Years 1926 through 2003 were used for stream-flow validation, based on data availability for both climate and stream-flow data. RHESSys estimates of daily trajectories of percentage basin snow cover during the melt period for years 2001 to 2004 with estimates derived from MODIS were also compared. For simulation analyses of spatiotemporal patterns of transpiration, RHESSys was used to compute:

(1) average basin transpiration from years 1926–2003 and (2) transpiration for 54 different elevation zones for water years 1990–2001. Data storage and computational efficiency issues required use of a shorter time span for spatial analysis. Elevation zones were 50 m each, ranging from 1200 to 3950 m. Patch-scale estimates of transpiration and other water flux estimates were averaged for each elevation zone.

The total area below 1850 m and above 3350 m was relatively small compared to the rest of the basin: 88% of the basin had elevations ranging from 2100 to 3350 m. There were relatively equal proportions of north, south, east, and west facing slopes, with large variations in aspect occurring in the 1350 to 1750 m range, and few east-facing slopes at the highest elevations. A test to determine if spatial differences in transpiration could be attributed to the orientation of the slope was conducted. Individual patches were classified into north, south, east, and west facing slopes, and mean annual transpiration for 1996 (a year with average air temperatures and precipitation) was calculated for each direction for the entire basin.

Climate Indices

Annual and seasonal climate indices were created to examine the relationship between simulated annual transpiration and climate variation, at both basin and sub-basin (elevation zones) scales. The set of annual and seasonal climate indices used in this study were formatted after Case and Peterson (2005), who identified climate indices that showed significant relationships with annual growth in western mountain environments. These, include: water year total precipitation, water year average air temperature, day of year when snowdepth decreased to zero, growing season maximum air temperature, growing season average air temperature, growing season precipitation, and peak 15-day running average of snowpack depth calculated from meteorological data from the Yosemite station (which represents a basin average snow depth and not delineated for different elevation zones). A water year was defined as October through September and growing season defined as May through September. Linear and polynomial regressions were calculated between climate indices and water year total transpiration to determine which indices had the largest effect on transpiration at the basin-scale. The relationship between climate indices and within-basin spatial variation in transpiration (measured as coefficient of variation (CV)) was also examined. Based on the basin-scale regressions, annual precipitation, growing season maximum air temperature, and peak 15-day running average snow depth were used to explore transpiration patterns within basin defined by patches and elevation intervals.

Difference maps were created to depict spatial patterns of the relative sensitivity of transpiration to climate variation. Based on results from spatial analyses, transpiration differences were computed for (a) years with the highest versus lowest growing season maximum air temperature, (b) highest versus average annual precipitation,

Table I. Calibration parameter set

	K (m day ⁻¹)	m (m day ⁻¹)	gw1 0–1	gw2 0–1	Error (%)	NS	Logged NS
Calibration	60	3.6	0.29	0.33	12	0.71	0.72
Validation	60	3.6	0.29	0.33	11	0.67	0.77

Note: saturated hydraulic conductivity (K), decay of K with depth (m), freshwater to groundwater (gw1), and groundwater to stream-flow (gw2). Error represents the percentage error of modelled from observed stream-flow. Daily (NS) and log-transformed daily (logged NS) stream-flow Nash–Sutcliffe efficiency results from correspondence between observed and modelled stream-flow.

and (c) lowest versus average annual precipitation. Years chosen for analyses were based on basin scale means of climate data, where 1998 and 2001 were the lowest and highest years of growing season mean air temperature, and 1998 and 1994 were the highest and lowest precipitation years, with 2000 having moderate precipitation.

RESULTS

Calibration and Validation

The parameter set selected from the calibration (Table I) was able to capture major hydrologic trends, based on Nash–Sutcliffe efficiency for daily and log-transformed daily stream-flow (71 and 72% efficiency, respectively). Error in estimating mean annual stream-flow for the calibration period was 12%. For the validation period (1926–2003), simulated mean annual stream-flow differed from observed values by only 11% (Figure 3) and Nash–Sutcliffe performance measures were 67 and 77% for daily and log-transformed daily stream-flow (Table I). The model did well at capturing timing of onset and end of seasonal stream-flow, but was slightly off in some estimates of peak stream-flow. Comparison between RHESSys estimates and MODIS estimates of percentage basin snow coverage resulted in an R^2 of 0.95.

Basin Scale Transpiration–Climate Relationships

Simulated average annual transpiration, from years 1929 to 2003 for the Upper Merced basin, was 418 mm, ranging from 279 to 547 mm. A distinct seasonal pattern of daily transpiration exists with transpiration decreasing to nearly zero in mid-November, values increasing in

early February, and peaks in late June (Figure 4). The climate indices with the greatest effect on total annual transpiration (basin average) were annual maximum 15-day running average snow depth (MXSN) and annual precipitation (APR), based on a polynomial regression (second order) ($R^2 = 0.32$ and 0.29 , respectively, $p < 0.001$) (Table II). A lag effect existed between previous year climate indices and accumulated transpiration, but the significance was not as strong as compared with climate indices from the same water year (based on linear regressions, polynomial regressions were not significant) (Table II). MXSN depth and annual precipitation in this basin were highly correlated ($R^2 = 0.97$, $p < 0.001$). Ninety-five per cent of precipitation at treeline falls as snow in this region (Stephenson, 1988; Melack and Stoddard, 1991), thus for the period of historic record snow and annual precipitation are interchangeable as predictors. Basin transpiration was lowest in the driest and wettest years, and highest in years of moderate precipitation levels, creating a unimodal relationship between transpiration and MXSN and ARP. No distinct trend occurred with growing season mean air temperature (GSMT) (Figure 5). The CV value reflects the degree of within-basin spatial variation in transpiration adjusted for the spatial mean. The CV value tends to increase for colder and wetter years (Figure 6).

Annual transpiration varied with aspect, but differences were not significant (Figure 7). The basin has a variety of different slopes and soil types within an aspect, which may affect why a statistically significant difference in north and south facing slopes was not detected. A multiple regression between elevation, aspect and annual transpiration was conducted, and it was found that

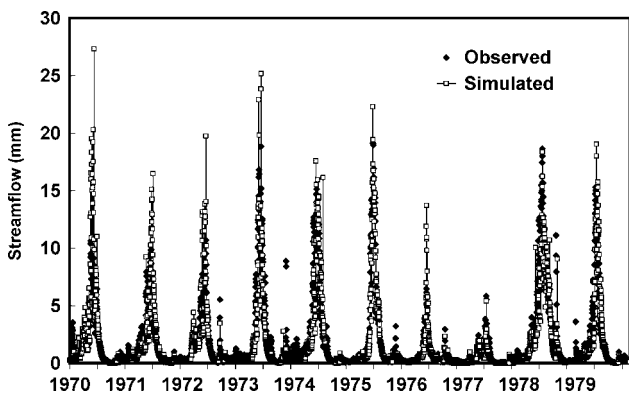


Figure 3. Daily simulated versus observed stream-flow patterns (in millimetres) for the 465 km² basin used in validation of RHESSys. Modelled stream-flow had a 6% error

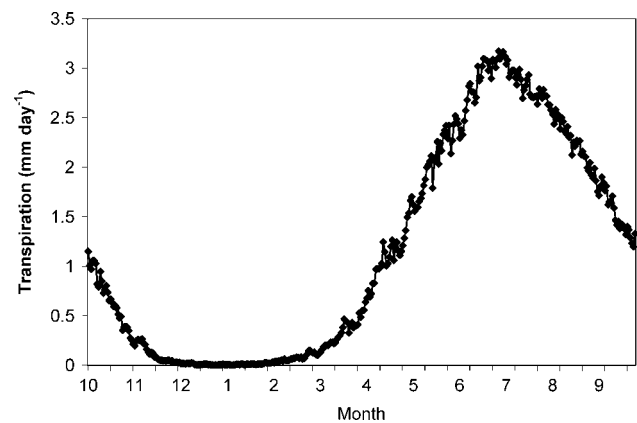


Figure 4. Averaged daily transpiration for a water year form 1929 to 2003 for the upper Merced watershed

Table II. The R^2 values from regressions of annual (water year) precipitation (APR), annual mean air temperature (AMT), day of year when snow reaches zero (Snow off), growing season maximum air temperature (GSMXT), growing season mean air temperature (GSMT), growing season precipitation (GSPR), and peak snow depth from a 15 day running average of snow depth (MXSN) on accumulated transpiration rates

	APR (mm)	AMT (°C)	Snow off (day)	GSMXT (°C)	GSMT (1st) (°C)	GSPR (mm)	MXSN (mm)
Acc Trans	0.289***	0.118	0.204***	0.162*	0.09** (+)	0.075	0.323***
Acc Trans(lag) (1st)	0.114**	0.006	0.092**	0.136**	0.002	0.017	0.099**
Variation	0.287***	0.065	0.269***	0.129	0.031 (+)	0.079	0.327***
CV (1st)	0.089** (+)	0.155*** (-)	0.143*** (+)	0.011 (-)	0.191*** (-)	0.004 (-)	0.103** (+)

Note: the p values refer to level of significance between transpiration variables and climate indices. "1st" represents linear regressions, remainder are 2nd order regressions.

*** $p < 0.001$.

** $p < 0.01$.

* $p < 0.1$.

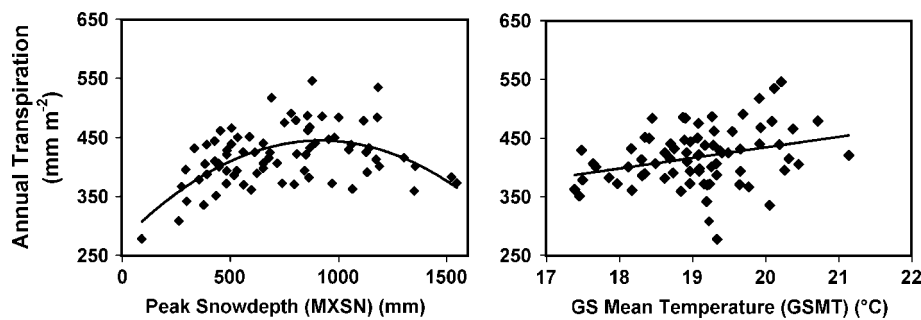


Figure 5. Simulated annual transpiration versus peak snow depth (MXSN) and growing season mean air temperature (GSMT) for the Merced River Basin for the period 1926 to 2003. Trend line represents a second order regression ($R^2 = 0.32$, $p < 0.001$ and $R^2 = 0.09$, $p < 0.01$, respectively)

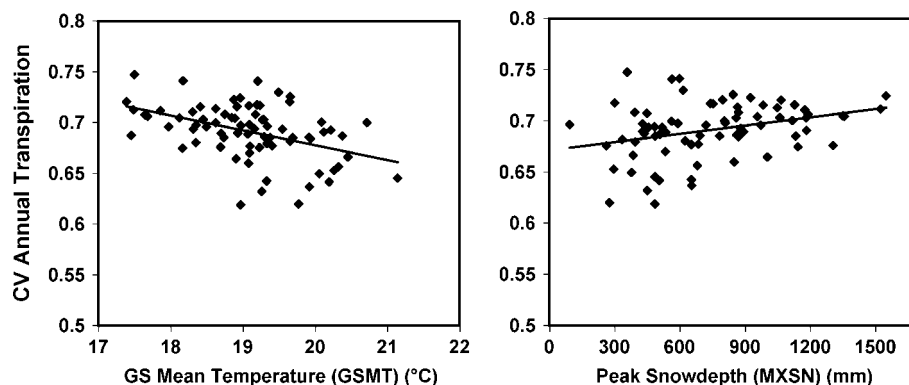


Figure 6. Coefficient of variation (CV) in basin growing season mean temperature (GSMT) annual transpiration versus peak in snow depth, $R^2 = 0.191$, $p < 0.001$ and $R^2 = 0.1$, $p < 0.01$, respectively)

elevation zones had a higher correlation to transpiration in this watershed ($R^2 = 0.35$, $p < 0.0001$) (Table II). These elevation zones showed strong spatial differences in transpiration (Figure 8a) and its response to climate variation.

Average annual transpiration was highest in riparian zones at the lowest elevations ($\sim 800 \text{ mm m}^{-2} \text{ year}^{-1}$). An area of steep cliffs between 1300–1700 m had little vegetation and thus low transpiration (Figure 8a). There was a broad range of transpiration rates at mid-elevations with values ranging from 450 up to 1012 $\text{mm m}^{-2} \text{ year}^{-1}$. Above 2700 m, transpiration decreased, and dropped to 0 $\text{mm m}^{-2} \text{ year}^{-1}$ at the highest elevations. To evaluate the extent to which these elevation differences in transpiration are due to differences in LAI, annual

transpiration for each elevation zone was normalized by its mean LAI (Figure 8b). Normalized transpiration showed a similar, though muted, trend with elevation. Thus elevational differences in transpiration can be attributed to differences in both vegetation (or ecosystem capacity for transpiration) and vegetation water use. Transpiration estimates, normalized by area (in mm m^{-2}), were used for data analyses.

The relationship between annual transpiration (normalized by drainage area but not LAI) and MXSN for separate elevation zones showed four distinct responses (Figure 9). Transpiration was insensitive to variability in MXSN at both low (1200–1800 m) and high (2600–4000 m) elevations and there was a wide range in annual transpiration rates, from 300–900 mm m^{-2}

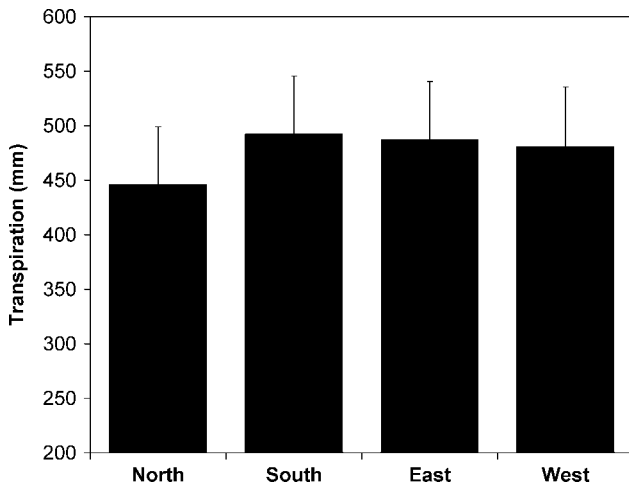


Figure 7. Means for averaged transpiration of 50 m elevation zones on north, south, east and west facing slopes of the Merced watershed. There was no significant difference between aspects

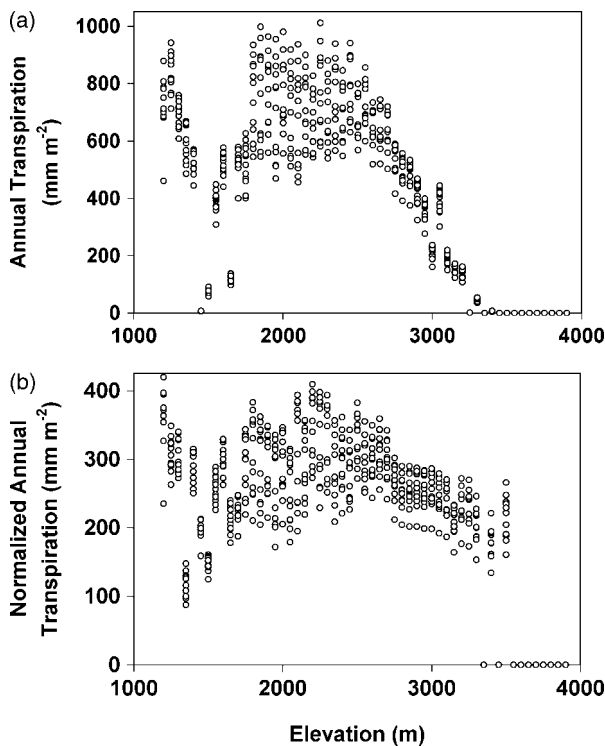


Figure 8. (a) Simulated annual transpiration from 50 m elevation zones for the basin ranging in elevation from 1200 to 4000 m. (b) Similar graph as (a) except with annual transpiration normalized by mean interval LAI values. Each dot represents 1 year of data for one 50 m elevation zone

year⁻¹ and 0–800 mm m⁻² year⁻¹ for the lowest and highest elevations, respectively (Figures 9a and 9d). In contrast, the lower-middle elevations (1800–2150 m) and higher-middle elevations (2150–2600 m) displayed distinct unimodal trends with MXSN, where transpiration peaked at MXSN levels of 881 mm m⁻² year⁻¹ (Figures 9b and 9c).

Transpiration in the lower-middle elevation range averaged 520 and 720 mm m⁻² year⁻¹ at low and high MXSN levels, respectively, and peaked at mid-MXSN at 1012 mm m⁻² year⁻¹ (Figure 9b). The higher-middle

elevations followed the same trend, with a less pronounced curve between low and high MXSN values. For both lower-middle and higher-middle elevations, departure from this unimodal trend with MXSN occurred in 1997 (MXSN = 1184 mm m⁻² year⁻¹) (data circled in Figures 9b and 9c). Mean annual air temperature was higher in 1997 (5.2 °C) as compared to temperatures in other years with similar values of MXSN (3.9 °C in 1998 with MXSN = 1191 mm m⁻² year⁻¹ and 4.6 °C with MXSN = 1144 mm m⁻² year⁻¹).

At the basin scale, GSMT was not significantly related to accumulated transpiration (Table III), but analysis within elevation zones revealed significant trends with GSMT (Figures 9e–9h). The lower elevations showed a positive significant trend with GSMT ($R^2 = 0.3$, $p < 0.001$) (Figure 9e). A significant positive relationship between transpiration and GSMT also occurred at the highest elevations of 2600 to 4000 m ($R^2 = 0.7$, $p < 0.001$) (Figure 9h), yet no significant relationship occurred at the middle elevations (Figure 9f and 9g).

Maps of the differences in transpiration between the maximum GSMT and minimum GSMT years across the basin show that greatest decreases in transpiration occurred in the lower-middle elevations, while higher elevations showed increased transpiration (Figure 10a). Note that the highest elevations showed little or no difference due to the high proportion of rock in these areas. Reductions in transpiration for a wet (highest APR, highest MXSN) versus average year were greatest at the higher-middle elevations (Figure 10b), whereas transpiration reductions in lowest versus average APR/MXSN years (Figure 10c) was greatest at lower-middle elevations.

The basin-scale impact of the response of transpiration to MXSN and GSMT depends on the proportional area of each elevation band (Figure 11). Middle elevation zones (1800–2600 m) contributed, on average, 51% of basin transpiration, with mid-high elevations (2150–2600 m) within this range contributing 29% of total transpiration. High elevation zones contributed, on average, 24% and low elevation zones 25% of total basin transpiration. The contribution of transpiration from middle elevations 1800 to 2600 m to basin totals increased with increasing MXSN until MXSN reached approximately 800 mm. The increases in relative contribution reflect the increase in transpiration rates with MXSN for these middle elevations (Figures 9b and 9c). At higher values of MXSN, although transpiration rates decrease for middle elevations, their relative contributions did not, since highest elevations also showed decreasing transpiration rates (Figures 9 and 11a). With higher air temperatures (higher GSMT), the relative contribution of middle elevations to total basin transpiration decreased reflecting a reduction in transpiration at low-middle elevations due to water stress (Figure 11b), and an increase in transpiration at the higher elevations (Figure 9h).

Table III. Summarized results from multiple regression analysis of annual transpiration against elevation and aspect

	Estimate	Standard error	<i>t</i> Value	<i>p</i> Value
(Intercept)	1204.9894	87.27899	13.806	<0.0001
Elevation (m)	-0.29531	0.02722	-10.85	<0.0001
Aspect (north, south, east, west)	9.81191	19.32305	0.508	0.612

Note: Elevation (50 m elevation zones) was significantly related to transpiration ($R^2 = 0.35$, $p < 0.0001$) while aspect (north, south, east, and west) was not significantly related.

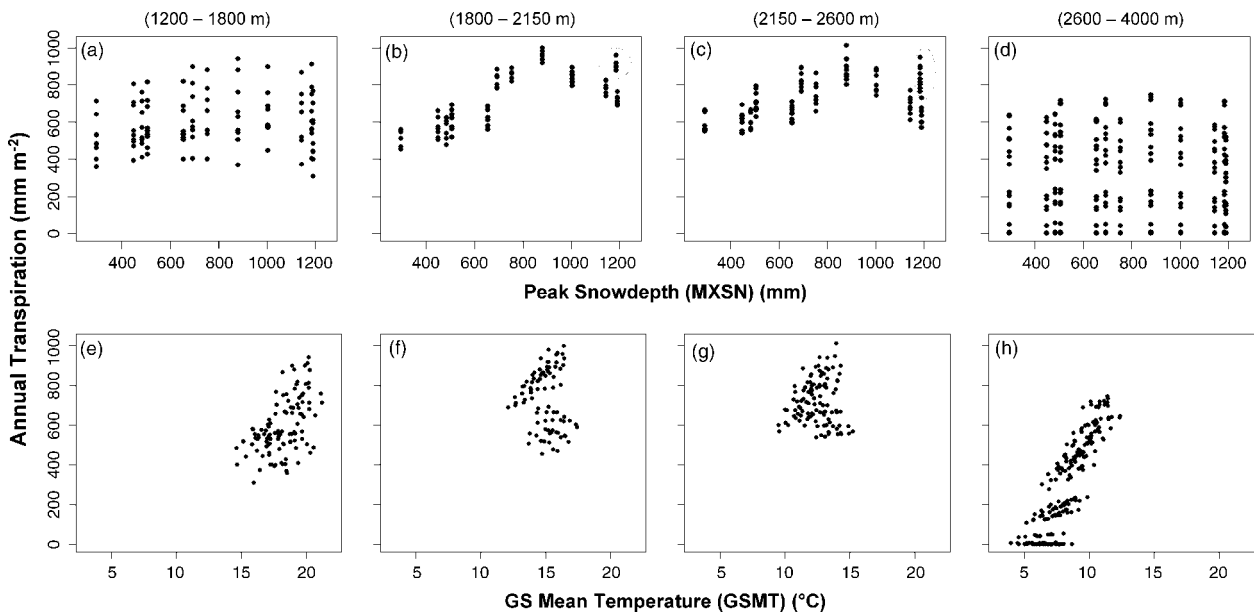


Figure 9. Simulated annual transpiration versus peak in snow depth (from 15 day running average) for each 50 m elevation range grouped from (a) 1200–1800, (b) 1800–2150 m, (c) 2150–2600 m and (d) 2600–4000 m. Graphs (e)–(h) define simulated annual transpiration versus growing season mean air temperature, divided into same elevation zones

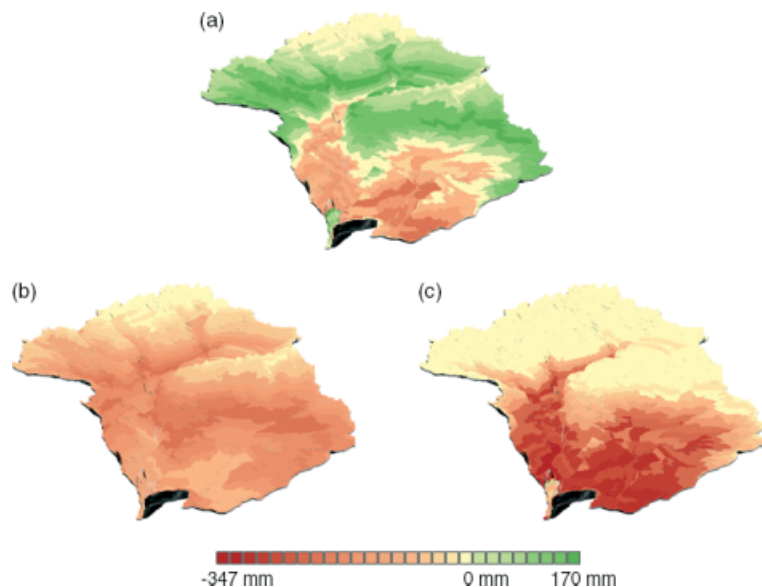


Figure 10. Three-dimensional maps of areas with greatest differences in transpiration between (a) warmest and coldest simulation years, (b) wet versus average precipitation year and (c) dry versus average precipitation year. Greatest decreases are depicted by dark grey (red) while increases in transpiration between years are defined by grey (green). The maps were rotated with the Happy Isles bridge stream gauge located at the bottom centre of the image

DISCUSSION

Use of a GIS-based dynamic model of coupled hydrological and ecological processes allowed us to examine

how relationships between climate, topography, and vegetation influence spatiotemporal patterns of transpiration. The results showed that the response of transpiration to climate at the basin scale was unimodal

where maximum transpiration rates occurred at moderate precipitation and snow depth (annual maximum) levels. While this response may seem intuitive based on the orographic nature of mountain ecosystems, within-basin details shed light on the varying climatic and topographic controls on basin scale transpiration rates.

Further division of the landscape into elevations zones suggested four trends of transpiration patterns along an elevational gradient. The first occurred in the lowest elevations where there was relatively little sensitivity of transpiration to year-to-year climate variation. This relationship follows hypotheses from Dunne *et al.* (2003), which predict a decoupling of plant function from snowmelt in lower elevations. Other investigators have reported similar patterns of plant response to climate. For example, forest growth patterns in the Pacific north-west showed insensitivity to climate variability at low elevations (Peterson and Peterson, 2001).

The second and third trends were within the intermediate elevation range, where there were two distinct classes of transpiration response to climate indices. Lower-middle elevations (1800–2150 m) showed strong sensitivity to water availability, resulting in a unimodal relationship between transpiration and annual precipitation and peak snow depth metrics. For years with little precipitation, transpiration was low due to water stress. Years with high precipitation also had low transpiration, which can be attributed to air temperature related limits on transpiration. The highest transpiration was seen at

moderate precipitation levels, which reflect the combined effect of contrasting controls on transpiration.

The third trend, which included slightly higher elevations within the middle elevation range (2150–2600 m), also illustrated transpiration as having a unimodal response to precipitation. Water availability was a weaker limit on transpiration, due to later seasonal snow melts and water inputs throughout summer when radiation inputs are high. For these elevations, however, air temperature sensitivities were greater (Figure 9g versus Figure 9f, and Figure 10a) when compared with mid-to-low elevations. Other studies have shown a similar transition from water-limited responses at lower elevations to air temperature-limited responses at higher elevations in western mountain ecosystems, although again these studies focused on growth (Case and Peterson, 2005). At both the basin scale and for the intermediate elevation ranges, it was found that transpiration totals were reduced at both low and high precipitation levels, a non-linear relationship with precipitation that represents optimality between water stress and air temperature limitations on transpiration.

The fourth trend was at the highest elevations, where transpiration exhibited a high sensitivity to air temperature and low sensitivity to precipitation, reflecting low vegetation biomass or the ecosystems' capacity to utilize available water inputs and energy. At these elevations, lower air temperatures limited model estimates of summer transpiration by reducing physiological rates (including stomatal conductance) as well as being indicative of reduced vapour pressure deficits. Other studies have also found plant functional response to air temperatures at high elevations (Dunne *et al.*, 2003; Walker *et al.*, 2006).

These trends in watershed transpiration give insight to differences in responses of particular zones. To examine how these patterns combined to affect total water budgets, transpiration estimates must be viewed in context of the relative amounts each zone attributes to the water balance. In the Merced basin, the moderate elevation classes dominated both in terms of area (51%) and transpiration rates. Consequently mean basin transpiration sensitivity to climate followed that of these moderate elevation classes. Changes in transpiration patterns had a much greater effect on the water budget at mid-elevations due to large relative size. The lowest maximum snow depth or highest growing season mean air temperatures brought about a 5% decrease in transpiration. This was partially compensated for by a higher percentage of basin transpiration at the highest elevations. But higher elevations comprise only 24% of the basin, so changes there did not have as large of an effect. In other basins, the distribution of basin area into elevational classes will differ. The Merced has a Mediterranean climate and is dominated by winter precipitation. Mountain forests in more continental climates might be less sensitive to changes in air temperature because soil water gets replenished periodically with summer rains. Therefore, the relative importance of the particular climate–transpiration relationships would change.

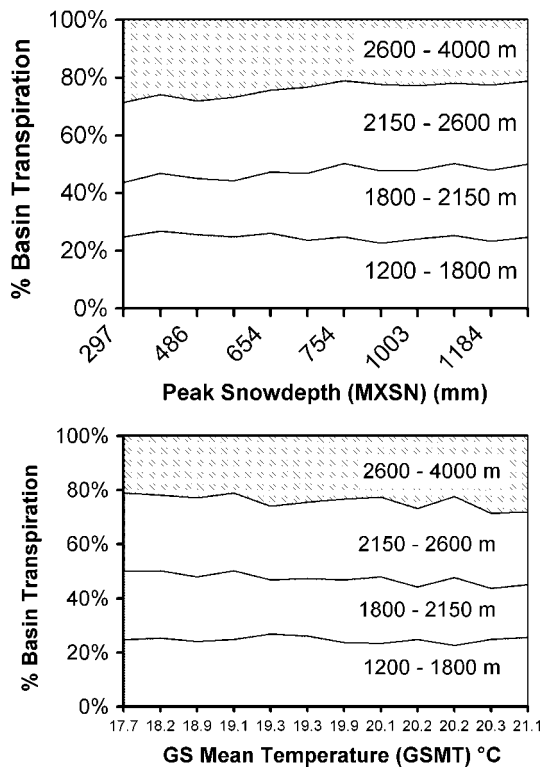


Figure 11. Proportion of annual transpiration contributed by four elevation ranges (1200–1800 m, 1800–2150 m, 2150–2600 m and 2600–4000 m) versus (a) peak in snow depth from 15 day running average and (b) growing season mean temperature

Comparison of years with extreme climate patterns showed large differences in transpiration (from years with maximum and minimum air temperature) occurred in the upper elevations as well as the lower-middle elevations (Figure 10a). These shifts could be indicative of larger scale changes in the water balance when coupled with changes in precipitation patterns. For the Merced, historic climate patterns show a high correlation between annual precipitation and peak snow metrics ($R^2 = 0.97$). Under a warmer climate, this correlation may weaken as more precipitation falls as rain, which would alter climate–transpiration relationships, particularly for middle elevations (Knowles *et al.*, 2006). Alteration of these relationships has further impacts on ecosystem processes, such as fire. Westerling *et al.* (2006) found climate to be a strong driver of wildfires in the western US, where middle elevations were more sensitive to fire due to earlier snowmelt timing. They found reduced winter precipitation was strongly associated with higher air temperatures. This affected summer drought which changed evapotranspiration patterns further affecting the flammability of live and dead fuels.

The spatiotemporal aspects of the model allowed us to address patterns of transpiration across a watershed, but limitations and uncertainty exist due to the nature of modelling. The use of dominant vegetation type and aggregation of species potentially decreased variability in transpiration rates, and these responses were confounded by other fine-scale controls, including rocks limiting vegetation growth. During time of stress, plants become vulnerable to shifts in biogeochemical patterns and/or species composition change (Ridolfi *et al.*, 2000; Jackson *et al.*, 2001), and these options were not included in the model given the relatively short (decadal) time frame of this study. Future work will explore these relationships.

In summary, this model based study illustrated the spatial complexities involved in assessing transpiration responses to variability and climate change. By providing a conceptual framework for assessing spatial patterns, model results can be used to focus field experimentation, additional modelling, and subsequent monitoring. For example, simulating the response of transpiration across a basin to varying energy, water availability, atmospheric conditions, vegetation, and topography allowed the identification of where ecosystem function within a basin was most sensitive to climate fluctuations. The information can be used to define areas with higher vulnerabilities to shifts in climate. Future efforts will conduct similar studies for cross-watershed comparison across the western US, examining not only transpiration patterns with varying climate (Mediterranean versus continental), but also changes in soil moisture, stream-flow, and other ecological functions in relation to climate change.

ACKNOWLEDGEMENTS

This research is a product of the Western Mountain Initiative, funded by the USGS under contract

04CRAG0004/4004CS0001, and EPA STAR grant Agreement Number: R829640. The authors thank two anonymous reviewers, Don McKenzie, and David L. Peterson for comments, and Richard Menicke for graphic support.

REFERENCES

- Aerial Information Systems. 2003. Comprehensive mapping classification: Yosemite and environs mapping classification and photo interpretation aid. Unpublished report submitted to the National Park Service: Washington, DC; 280.
- Bachelet D, Neilson RP, Lenihan M, Drapek RJ. 2001. Climate change effects on vegetation distribution and carbon budget in the United States. *Ecosystems* **4**: 164–185.
- Bales RC, Molotch NP, Painter TH, Dettinger MD, Rice R, Dozier J. 2006. Mountain hydrology of the western United States. *Water Resources Research* **42**: W08432. DOI: 10.1029/2005WR004387.
- Band LE, Patterson P, Nemani R, Running SW. 1993. Forest ecosystem processes at the watershed scale: incorporating hillslope hydrology. *Journal of Hydrology* **63**: 93–126.
- Band LE, Tague CL, Groffman P, Belt K. 2001. Forest ecosystem processes at the watershed scale: hydrological and ecological controls of nitrogen export. *Hydrological Processes* **15**: 2013–2028.
- Band LE, Mackay DS, Creed IF, Semkin R, Jeffries D. 1996. Ecosystem processes at the watershed scale: sensitivity to potential climate change. *Limnology and Oceanography* **41**: 928–938.
- Barry RG. 1992. *Mountain Weather and Climate*. Routledge: New York; 402.
- Boisvenue C, Running SW. 2006. Impacts of climate change on natural forest productivity—evidence since the middle of the 20th century. *Global Change Biology* **12**: 862–882.
- Case MJ, Peterson DL. 2005. Fine-scale variability in growth-climate relationships of Douglas-fir, North Cascade Range, Washington. *Canadian Journal of Forest Research* **35**: 2743–2755.
- Clow DW, Mast MA, Campbell DH. 1996. Controls on surface water chemistry in the upper Merced river basin, Yosemite National Park, California. *Hydrological Processes* **10**: 727–746.
- Clow DW, Schrott L, Webb R, Campbell DH, Torizzone A. 2003. Ground water occurrence and contributions to streamflow in an alpine catchment, Colorado Front Range. *Ground Water* **41**: 937–950.
- Dale VH, Joyce LA, McNulty S, Neilson RP, Ayres MP, Flannigan MD, Hanson PJ, Irland LC, Lugo AE, Peterson CJ, Simberloff D, Swanson FJ, Stocks BJ, Wotton BM. 2001. Climate change and forest disturbances. *BioScience* **51**: 723–734.
- Dettinger MD, Cayan DR. 1995. Large-scale atmospheric forcing of recent trends toward early snowmelt runoff in California. *Journal of Climate* **8**: 606–623.
- Dettinger MD, Cayan DR, Meyer MK, Jeton AE. 2004. Simulated hydrologic response to climate variations and change in the Merced, Carson, and American River basins, Sierra Nevada, California, 1900–2099. *Climatic Change* **62**: 283–317.
- Diaz HF. 2005. Monitoring climate variability and change in the western United States. In *Global Change and Mountain Regions, an Overview of Current Knowledge*, UM Huber HKM Bugmann MA Reasoner (eds). Springer: Dordrecht; 267–274.
- Dirnböck TN, Grabherr DG. 2000. GIS assessment of vegetation and hydrological change in a high mountain catchment of the Northern Limestone Alps. *Mountain Research and Development* **20**: 172–179.
- Dunne JA, Harte J, Taylor KJ. 2003. Subalpine meadow flowering phenology responses to climate change: integrating experimental and gradient methods. *Ecological Monographs* **73**: 69–86.
- Eder G, Fuchs M, Nachtnebel HP, Loibl W. 2005. Semi-distributed modeling of the monthly water balance in an alpine catchment. *Hydrological Processes* **19**: 2339–2360.
- Gurtz J, Lang H, Verbunt M, Zappa M. 2005. The use of hydrological models for the simulation of climate change impacts on mountain hydrology. In *Global Change and Mountain Regions, an Overview of Current Knowledge*, Huber UM, Bugmann HKM, Reasoner MA (eds). Springer: Dordrecht; 343–354.
- Heddeland I, Lettenmaier DP. 1995. Hydrological modeling of boreal forest ecosystems. In *Water Resource Series 14*, Department of Civil Engineering, University of Washington: Seattle, WA.
- Jackson RB, Carpenter SR, Dahm DN, McKnight DM, Naiman R, Postel SL, Running SW. 2001. Water in a changing world. *Ecological Applications* **11**: 1027–1045.

- Jarvis P. 1976. The interpretations of the variations in leaf water potential and stomatal conductance found in canopies in the field. *Philosophical Transactions Series B* **273**: 593–610.
- Kane DL. 2005. High-latitude hydrology, what do we know? *Hydrological Processes* **19**: 2453–2454.
- Kang S, Lee D, Lee J, Running SW. 2006. Topographic and climatic controls on soil environments and net primary production in a rugged temperate hardwood forest in Korea. *Ecological Research* **21**: 64–74.
- Knowles N, Dettinger MD, Cayan DR. 2006. Trends in snowfall versus rainfall for the Western United States. *Journal of Climate* **19**: 4545–4559.
- Loik ME, Redar SP, Harte J. 2000. Photosynthetic responses to a climate-warming manipulation for contrasting meadow species in the Rocky Mountains, Colorado, USA. *Functional Ecology* **14**: 166–175.
- Mast MA, Clow DW. 2000. *Environmental Characteristics and Water Quality of Hydrologic Benchmark Network Stations in the Western United States, US Geological Survey Circular 1173-D*. US Geological Survey: Reston, VA.
- Melack JM, Stoddard JL. 1991. Sierra Nevada, California. In *Acidic Deposition and Aquatic Ecosystems—Regional Case Studies*, DF Charles (ed.). Springer Verlag: New York; 503–530.
- Monteith JL. 1965. Evaporation and environment, the state and movement of water in living organisms. In *Proceedings of the 19th Symposium, Society of Experimental Biology*. Cambridge University Press: London; 205–234.
- Mote PW, Hamlet AF, Clark MP, Lettenmaier DP. 2005. Declining mountain snowpack in western North America. *Bulletin of the American Meteorological Society* January: 39–49.
- Nash J, Sutcliffe J. 1970. River flow forecasting through conceptual models: Part 1—a discussion of principles. *Journal of Hydrology* **10**: 282–290.
- Nemani R, White M, Thornton P, Nishida K, Reddy S, Jenkins J, Running S. 2002. Recent trends in hydrologic balance have enhanced the terrestrial carbon sink in the United States. *Geophysical Research Letters* **29**(10): 1468. DOI: 10.1029/2002GS014867.
- Nishida K, Nemani RR, Glassy JM, Running SW. 2003. Development of an evapotranspiration index from Aqua/MODIS for monitoring surface moisture status. *IEE Transactions on Geoscience and Remote Sensing* **41**: 493–501.
- National Soil Survey Characterization Data (NSSCD). 2006. *Soil Survey Staff 2006*. National Soil Survey Characterization Data, Soil Survey Laboratory, National Soil Survey Center, USDA-NRCS: Lincoln, NE; Wednesday, May 24, 2006.
- Parton WJ, Mosier A, Ojima D, Valentine D, Schimel D, Weier K, Kulmala A. 1996. Generalized model for N₂ and N₂O production from nitrification and denitrification. *Global Biogeochemical Cycles* **10**: 401–412.
- Pan Z, Arritt RW, Takle ES, Gutowski WJ Jr., Anderson CJ, Segal M. 2004. Altered hydrologic feedback in a warming climate introduces a 'warming hole'. *Geophysical Research Letters* **31**: L17109. DOI: 10.1029/2004GL020528.
- Peterson DW, Peterson DL. 2001. Mountain hemlock growth responds to climatic variability at annual and decadal time scales. *Ecology* **82**: 3330–3345.
- Pupacko A. 1993. Variations in Northern Sierra Nevada streamflow: implications of climate change. *Water Resources Bulletin* **29**: 283–290.
- Rademacher LK, Clark JF, Hudson GB, Erman DC, Erman NA. 2001. Chemical evolution of shallow groundwater as recorded by springs, Sagehen basin, Nevada County, California. *Chemical Geology* **179**: 37–51.
- Ridolfi L, D'Odorico P, Porporato A, Rodriguez-Iturbe I. 2000. Duration and frequency of water stress in vegetation: an analytical model. *Water Resources Research* **36**: 2297–2307.
- Running R, Nemani R, Hungerford R. 1987. Extrapolation of synoptic meteorological data in mountainous terrain and its use for simulating forest evapotranspiration and photosynthesis. *Canadian Journal Forest Research* **17**: 472–483.
- Shär C, Frei C. 2005. Orographic precipitation and climate change. In *Global Change and Mountain Regions, an Overview of Current Knowledge*, Huber UM, Bugmann HKM, Reasoner MA (eds). Springer: Dordrecht; 255–266.
- Sierra Nevada Ecosystem Project (SNEP). 2005. Available at <http://ceres.ca.gov/snep/pubs/index.html>. [accessed January 2006].
- Stephenson NL. 1988. *Climatic control of vegetation distribution—the role of the water balance with examples from North America and Sequoia National Park, California*. PhD thesis, Cornell University, Ithaca, NY.
- Stewart IT, Cayan DR, Dettinger MD. 2004. Changes in snowmelt runoff timing in Western North America under a 'business and usual' climate change scenario. *Climatic Change* **62**: 217–232.
- Tague CL, Band LE. 2001. Evaluating explicit and implicit routing for watershed hydro-ecological models of forest hydrology at the small catchment scale. *Hydrological Processes* **15**: 1415–1439.
- Tague CL, Band LE. 2004. Regional hydro-ecologic simulation system: an object-oriented approach to spatially distributed modeling of carbon, water and nutrient cycling. *Earth Interactions* **8**: 1–42.
- Tague CL, Farrell M, Grant G, Choate J, Jefferson A. 2008. Deep groundwater mediates streamflow response to climate warming in the Oregon Cascades. *Climatic Change* (in press).
- Thornton PE. 1998. *Regional ecosystem simulation: combining surface and satellite based observations to study linkages between terrestrial energy and mass budgets*. PhD thesis, School in Forestry, University of Montana, Missoula, MT.
- van Lier QD, Sparovek G, Flanagan DC, Bloem EM, Schnug E. 2005. Runoff mapping using WEPP erosion model and GIS tools. *Computers and Geosciences* **31**: 1270–1276.
- Walker MD, Wahren CH, Hollister RD, Henry GHR, Ahlquist LE, Alatalo JM, Bret-Harte MS, Calef MP, Callaghan TV, Carroll AB, Epstein HE, Jónsdóttir IS, Klein JA, Magnusson B, Molau U, Oberbauer SF, Rewa SP, Robinson CH, Shaver GR, Suding KN, Thompson CC, Tolvanen A, Totland O, Turner PL, Tweedie CE, Webber PJ, Wookey PA. 2006. Plant community responses to experimental warming across the tundra biome. *Proceedings of the National Academy of Science* **103**: 1342–1346.
- Westerling AL, Hidalgo HG, Cayan DR, Swetnam WA. 2006. Warming and earlier spring increase Western U.S. forest wildfire activity. *Science* **313**: 940–943.
- White MA, Thornton PE, Running SW, Nemani RR. 2000. Parameterization and sensitivity analysis of the BIOME-BGC terrestrial ecosystem model: net primary production controls. *Earth Interactions* **4**: 1–85.
- Wigmosta JA, Vail L, Lettenmaier DP. 1994. Distributed hydrology-vegetation model for complex terrain. *Water Resources Research* **30**: 34–46.
- Wilson KB, Hanson PJ, Mulholland PJ, Baldocchi DD, Wullschlegel SD. 2001. A comparison of methods for determining forest evapotranspiration and its components: sap-flow, soil water budget, eddy covariance and catchment water balance. *Agricultural and Forest Meteorology* **106**: 153–168.
- Whitaker A, Alila Y, Beckers J, Toews D. 2003. Application of the Distributed Hydrology Soil Vegetation model to Redfish Creek, British Columbia: model evaluation using internal catchment data. *Hydrological Processes* **17**: 199–224.

APPENDIX A

Classification of vegetation map

1	Hardwoods	<i>Quercus</i> sp., <i>Acer</i> sp. (Canyon Live Oak, Black Oak, Bigleaf Maple)
2	Aspen	<i>Populus tremuloides</i>
3	Pine	<i>Pinus contorta</i> (Lodgepole Pine), <i>Pinus ponderosa</i> (Ponderosa Pine), <i>Pinus jeffreyi</i> (Jeffrey Pine), <i>Pinus monticola</i> (Western White Pine), <i>Pinus albicaulis</i> (Whitebark Pine)
4	Fir/Hemlock/ other	<i>Pseudotsuga menziesii</i> (Douglas fir), <i>Tsuga mertensiana</i> (Mountain hemlock), <i>Abies magnifica</i> (red fir), <i>Abies concolor</i> (white fir)
5	Juniper	<i>Juniperus</i> sp.
6	Shrub vegetation	Includes Bush Chinquapin alliance, Huckleberry Oak alliance, Greenleaf Manzanita association
7	Sagebrush	<i>Artemisia</i> sp. (Mountain and Rothrock Sagebrush)
8	Willow	<i>Salix</i> sp. (Greyleaf Sierra Willow, Shrub Willow)
9	Grass	Sedge, graminoids
10	Herbaceous	Forbs
11	Conifer reproduction	Lower leaf area and lower woody fragmentation rate than Pine classification
12	Non-vegetation rock	Rock, talus, scree, sparse/non-vegetated rock, urban
13	Snow	
14	Water	
